Oxidative Molecular Layer Deposition of Amine-Containing Conjugated Polymer Thin Films

Quinton K. Wyatt, ¹ Mitchel Vaninger, ² Nikhila C. Paranamana, ¹ Thomas W. Heitmann, ^{2,3} Helmut Kaiser, ³ Matthias J. Young, ^{1,4,5*}

Abstract

Conjugated polymers such as polyethylenedioxythiophene (pEDOT), polypyrrole (pPy), and polyaniline (pAni) exhibit high electrochemical capacities, making them appealing as electrode materials for energy storage, electrochemical desalination, and chemical sensing. Recent work has established the growth of thin films of pEDOT using alternating gas-phase exposures of the EDOT monomer and a metal-chloride (e.g. MoCl₅) oxidant in a process termed oxidative molecular layer deposition (oMLD). Here, we describe the first demonstration of oMLD of aminecontaining conjugated polymers. We find that pyrrole (Py) and MoCl₅ undergo self-limiting surface reactions during oMLD exposures to form conformal pPy thin films, but oMLD using aniline (Ani) and p-phenylenediamine (PDA) monomers yields unexpected azo functionality. The formation of azo groups is attributed to an MoCl₅-amine surface adduct that spatially constrains polymerization reactions near the amine group and produces azo groups when coupling two primary amines. pPy grown by oMLD exhibits a record-breaking 282 mAh/g capacity in aqueous electrolyte, and PDA/MoCl₅ oMLD yields azo-polymers of interest as anode materials for alkaliion batteries. Alternating between Py and PDA monomers during oMLD produces molecularly assembled copolymers with qualitatively different electrochemical responses from the isolated monomer structures. This work lays the foundation for the growth of conformal thin films of conjugated amine polymers with molecular-level control of composition and thickness.

Keywords: Nanoscale Materials; Energy Storage; Desalination; Electrochemistry; Soft Materials;

¹Department of Chemistry, University of Missouri, Columbia, MO, 65211, USA

²Department of Physics and Astronomy, University of Missouri, Columbia, MO, 65211, USA

³Missouri Research Reactor, University of Missouri, Columbia, MO, 65211, USA

⁴Department of Biomedical, Biological and Chemical Engineering, University of Missouri, Columbia, MO, 65211, USA

⁵Materials Science and Engineering Institute, University of Missouri, Columbia, MO, 65211, USA *email: matthias.young@missouri.edu

Introduction

Conjugated polymers such as polyethylenedioxythiophene (pEDOT), polyaniline (pAni) and polypyrrole (pPy), are of interest for electrochemical energy storage, electrochemical desalination,² and chemical sensors.³ Heteroatoms in these polymers undergo reversible electrochemical redox reactions to switch between lone-pair and cation-radical configurations, yielding high electrochemical capacity.⁴ These redox reactions also produce charge carriers (electrons and holes) that travel down the conjugated backbone of these polymers to produce high electronic conductivities of 100-6,000 S/cm.⁵⁻⁸ Following the recent demonstration of desalination batteries^{9,10} and anion-based batteries,^{11,12} these conjugated polymers are also of interest for their ability to reversibly bind anions from solution during electrochemical cycling. Under positive potentials, cation-radicals form on the polymer backbone that attract and bind anions. pAni and pPy are two of the most well-studied polymers in this class, initially discovered more than 150 years ago. ^{13,14} Compared with pEDOT, which contains S and O heteroatoms, polymers containing N heteroatoms (amine groups) such as pAni and pPy are lower cost, more environmentally friendly, and have higher theoretical charge storage capacities. Assuming one electron redox per monomer, pAni has a theoretical capacity of 294 mAh/g and pPy has a theoretical capacity of 411 mAh/g. These values exceed the theoretical capacities for some of the most promising electrode materials for next-generation alkali ion batteries, 15,16 and promise to enable high-energy-density polymer batteries made from earth-abundant elements (i.e. C, N, H).

Unfortunately, traditional approaches for conjugated amine polymer synthesis struggle to achieve these maximum theoretical capacities, with the highest experimental capacities limited to ~150 mAh/g.⁴ These lower experimentally achieved capacities are thought to arise from (1) irreversible formation of electrically resistive phases during electrochemical cycling^{17,18} and (2) non-ideal local molecular structures.¹⁹ We also note that anions diffuse slowly through these polymers (solid state diffusivity of ~10⁻¹⁵ cm²/s at room temperature), introducing overpotentials in bulk polymers or thick polymer films and leading to lower capacities.^{20–22} However, these issues are not intrinsic to the polymer materials and could be overcome with improved synthesis approaches. For example, delivering polymer thin films with controlled molecular structures onto a conductive (e.g. carbon) support would be expected to overcome these shortcomings and allow for higher electrochemical capacities.

However, controlling the molecular structure and thickness of conjugated polymer films is challenging using established synthesis approaches. Conjugated polymer synthesis is traditionally performed by solution-phase homogeneous chemical oxidation using chemical oxidants such as ammonium persulfate (APS) or Iron(III) chloride (FeCl₃).²³ The polymerization process is initiated through chemical oxidation of monomers, followed by quenching with other monomers and short chain oligomers to form a varied distribution of metastable branched structures.^{24–26} Furthermore, this synthesis approach does not easily allow for formation of polymer films – instead yielding irregularly-shaped particles or nanofibers,^{27,28} which must be dissolved, e.g. in m-cresol, and spin-coated to produce rough (> 1 μm roughness) films.^{29,30} This approach is not easily applied to 3D substrates. Synthesis of these polymers can also be achieved using electrodeposition, which provides some control over polymer film thickness, e.g. by pulse deposition,^{31,32} but this approach suffers from similar challenges regarding molecular structure control, and electrodeposition onto porous substrates is challenging.^{33,34}

Over the last 30 years, research into vapor-phase polymerization (VPP) has established the groundwork to form conformal thin films of conjugated polymers with control over molecular structure. ^{35–37} Early work in this area focused on mixing a monomer and oxidant homogeneously in the gas-phase. As the gas-phase polymer chains increase in length, they condense onto a substrate surface in a process termed oxidative chemical vapor deposition (oCVD). This oCVD process employing homogenous gas-phase mixing has been demonstrated for pPy, ³⁸ pAni, ³⁹ and pEDOT, ⁸ yielding improved electrical conductivity for pEDOT relative to solution-phase polymerization due to the absence of side-chains or additives needed for solution processing. ⁷ While oCVD provides improved control over the uniformity and thickness of conjugated polymer films, it is a line-of-sight technique that provides poor uniformity on 3D supports, ⁴⁰ and oCVD is not expected to provide improved molecular structure control as it also employs homogeneous oxidation (albeit in the gas phase).

More recently, studies have improved on the oCVD process to provide a route for more pristine control over molecular structure and thickness. To achieve this, the gas phase precursors used in oCVD are separated and delivered as alternating chemical exposures separated by an inert purge step in a process termed oxidative molecular layer deposition (oMLD).^{41,42} oMLD stems conceptually from atomic layer deposition (ALD)^{43–45} and is an extension of the sub-class of ALD

known as molecular layer deposition (MLD). 46-49 In ALD, organometallic precursors and coreactants (e.g. water) are dosed in sequential gas-phase exposures and undergo self-limiting (typically ligand exchange) surface reactions to produce thin films with atomic-scale control of thickness. MLD is analogous to ALD, but employs complementary bifunctional organic molecules in sequential gas-phase exposures to grow polymer films. For example, alternating exposures of adipoyl chloride (a bifunctional acyl halide) with 1,6 hexanediamene (a bifunctional primary amine) react to form R-C-O-N-C-R linkages at the surface and produce the nylon 66 polymer. 49 The self-terminating surface reactions in MLD processes allow for the formation of uniform coatings on complex 3D surfaces. 42,50,51 oMLD is similar to conventional MLD, but employs alternating exposures of a monomer and *gas-phase chemical oxidant* to drive surface-based radical polymerization reactions. To date, pEDOT is the only polymer that has been demonstrated using the oMLD technique. 41,52,53

Here, we expand on previous studies of oMLD, ^{41,52,53} and present the first report of oMLD using a monomer other than EDOT – specifically we study the amine-containing monomers: pyrrole (Py), aniline (Ani), and paraphenylenediamine (PDA). Our objective in this work was to (1) establish controlled oMLD growth to form thin films of precise thickness, (2) understand the oMLD growth mechanisms for these chemistries, and (3) take advantage of the thickness control and mechanistic understanding to generate polymer films with controlled molecular structure and improved electrochemical properties. Through this effort, we gained new insights into the chemical mechanisms for oMLD and identified monomer-dependent differences in growth yielding unexpected polymer structures and electrochemical properties for oMLD films grown using amine-containing monomers.

Results and Discussion

Establishing oMLD Growth of Polypyrrole

Our initial studies focused on oMLD of Py. We first employed *in situ* quartz crystal microbalance (QCM) studies to examine whether sequential exposures of Py and MoCl₅ result in self-limiting and controlled growth. Figure 1 depicts steady-state QCM results for oMLD growth of Py/MoCl₅ at 100 °C using an 8 s Py dose, 200 s Ar purge, 55 s MoCl₅ dose, and 200 s purge for each oMLD cycle. The linear growth we observe in Figure 1a is a hallmark of controlled ALD and

MLD growth behavior. This linear growth arises from self-limiting surface reactions for each precursor exposure. In Figure 1b and 1c, we show average QCM traces during MoCl₅ and Py doses, respectively. These QCM data are average traces over five cycles at steady state following 50 oMLD cycles. The leveling-off of the mass change during each precursor exposure is consistent with self-limiting reaction behavior.

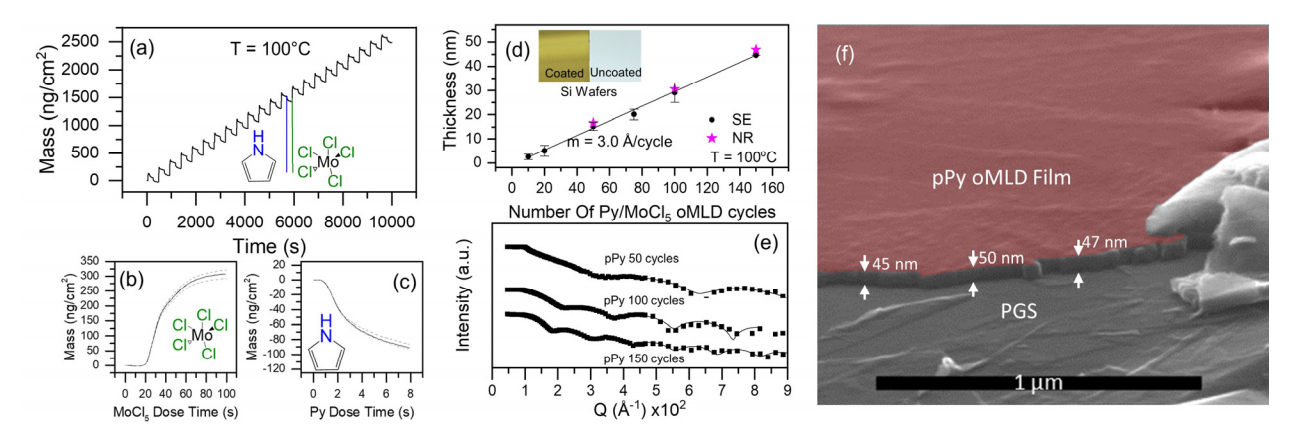


Figure 1. Demonstration of self-limiting and linear growth of Py/MoCl₅ oMLD at 100 °C including (a) QCM during 22 Py/MoCl₅ oMLD cycles, (b) QCM mass change during MoCl₅ dose averaged over 5 oMLD cycles at steady-state, (c) QCM mass change during Py dose averaged over 5 oMLD cycles at steady-state, (d) thickness vs. number of Py/MoCl₅ oMLD cycles as measured by SE and NR with inset showing photographs of Si coated with 100 oMLD cycles of Py/MoCl₅ vs. uncoated Si wafer, and (e) raw NR data for 50, 100, and 150 oMLD cycles of Py/MoCl₅ including model fits corresponding to thicknesses shown in (d). Also shown (f) is SEM imaging (colorized) of cleaved PGS with pPy oMLD film formed by 150 Py/MoCl₅ oMLD cycles at 100 °C showing uniform conformal coating.

Based on the linear growth and saturating exposures observed from *in situ* QCM studies in Figure 1a-c, we expect to be able to control film thickness of pPy films by adjusting the number of Py/MoCl₅ oMLD cycles. To confirm this, we performed varying numbers of oMLD cycles on silicon (Si) wafers and evaluated the resulting film thickness *ex situ* using spectroscopic ellipsometry (SE) and neutron reflectivity (NR). In Figure 1d, we observe a linear increase in film thickness with an increasing number of oMLD growth cycles—as expected for controlled MLD growth. A linear fit of the SE data in Figure 1d yields a growth rate of 3.0 Å/cycle. This

corresponds closely to the diameter of a Py monomer of 3.91 Å, 54,55 and indicates that \sim 0.8 monolayers of pPy are formed per oMLD growth cycle at 100 °C.

We also show the raw NR data (background subtracted, footprint corrected, and normalized) with model fits for select pPy films in Figure 1e. These NR data show an increased number of Kiessig fringes over the same Q-range with an increased number of oMLD cycles, indicating an increased film thickness. The well-defined Kiessig fringes are indicative of smooth films, where modeling of this NR data yielded an RMS roughness of 0.86 nm for a 46.2 nm thick film (150 oMLD cycles). The NR and SE thicknesses agree closely in Figure 1d. In Figure 1f, we also confirmed by scanning electron microscopy (SEM) that the thickness of oMLD films deposited on Si wafers in Figure 1d is consistent with films formed on pyrolytic graphite sheet (PGS) carbon substrates used for electrochemical measurements. In Figure 1f we measure a film thickness of 47 ± 2 nm for pPy on PGS after 150 Py/MoCl₅ oMLD cycles at 100 °C, which is in close agreement with the SE thickness of 44.7 nm measured on Si.

In the Supporting Information (SI) Section A, we also examine the effect of purge time on the uniformity of pPy oMLD films and identify that a purge time of ≥120 s is necessary to prevent uncontrolled oCVD through gas-phase mixing of Py and MoCl₅ precursors – hence the 200 s purge time used in Figure 1. Using sufficient purge times, we demonstrate oMLD pPy growth into trenches with a 200:1 aspect ratio in SI Section A. We note that dose and purge times employed here are optimized for a custom laboratory-scale reactor, and different reactor geometries and ALD-type deposition schemes such as spatial ALD⁵⁶ or fluidized-bed ALD⁵⁷ geometries could be employed to accelerate depositions on higher quantities of substrate (e.g. carbon powder) for scale-up and device deployment.

Combining the mass gain per cycle (MGPC) of 112 ng/cm²/cycle from steady state QCM in Figure 1a with the growth rate of 3 Å/cycle from *ex situ* SE and NR data in Figure 1d, we calculate a film density of 3.7 g/cm³. This value is higher than typical densities of 1.5 g/cm³ expected for pPy. ^{58,59} However, X-ray photoelectron spectroscopy (XPS) data (*see SI Section B*) indicates that MoCl_x residue remains in the oMLD pPy following deposition. Assuming the oMLD pPy/MoCl_x composite occupies the same volume as pure pPy polymer, but with one MoCl₃ molecular unit per Py monomer incorporated into the structure yields a density of 6.0 g/cm³. The density of 3.7 g/cm³ is therefore consistent with ~0.5 MoCl₃ molecules per Py monomer, in line with the Mo:N atomic ratios measured by XPS in SI Section B. We note that the MoCl_x residue is

electrochemically inert and is removed upon rinsing,⁴¹ and we therefore assume a density of 1.5 g/cm³ for the pPy films when calculating specific mass capacities from electrochemical experiments below (see Materials and Methods section for further details).

In Figure 2a we compare the cyclic voltammetry (CV) characteristics of oMLD pPy vs. electrodeposited pPy. The electrodeposited pPy film in Figure 2a was grown to a thickness of 30.4 nm (as measured by SE) on a gold electrochemical quartz crystal microbalance (EQCM) electrode using pulsed electrodeposition procedures reported previously. 66,67 The mass of the final pPy film measured via EQCM was 5.56 μg, corresponding to a density of 1.34 g/cm³. This electrodeposited pPy film exhibited a specific capacity of 128.4 mAh/g at a sweep rate of 50 mV/s, consistent with typical capacities of ~140 mAh/g reported for pPy. ^{4,69} The 20.4 oMLD pPy film in Figure 2a was deposited using 150 oMLD cycles at a growth temperature of 150 °C. The pPy thickness was measured via SE on Si wafers placed adjacent to each PGS sample in the reactor chamber. In Figure 1, we show close agreement between pPy thicknesses on Si and PGS. Multiplying the thickness by the electrode area (1.21 cm²), and assuming a density of 1.5 g/cm³ for pPy, we calculate a specific capacity of 258 mAh/g for the oMLD pPy film in Figure 2a. We note that the oMLD pPy film has a visibly higher current (in A/g) than the electrodeposited pPy, consistent with this higher capacity. We also note that the CV for the oMLD pPy is qualitatively different from the CV curve for electrodeposited pPy, and exhibits an additional redox peak at more oxidizing potential (+0.2 V vs. Ag/AgCl). We attribute the additional CV peak for oMLD pPy to the formation of different local structures within the pPy film, providing an enhanced electrochemical capacity. Specifically, we expect that MoClx residue within the pPy film helps to prevent pore collapse of the pPy polymer fibers and provide a higher electrochemical capacity.

We also performed CV on oMLD pPy films of 7.7 nm and 5.5 nm thickness deposited at 150 °C, and we measured specific capacities of 260 mAh/g and 247 mAh/g, respectively, at a sweep rate of 50 mV/s. All of the pPy film thicknesses exhibited reversible rectangular-shaped pseudocapacitive behavior, with a visible redox feature at an equilibrium potential of -0.2 V vs. Ag/AgCl—in agreement with the known electrochemical properties of pPy.⁶⁸ We expected that the thinnest pPy films would exhibit the best rate performance, and so we performed CV characterization at varying sweep rates for a series of samples formed together in the same deposition run where the average pPy thickness measured on all the samples in reactor chamber

was 5.5 ± 0.2 nm. In Figure 2b we report CV of the 5.5 nm pPy thickness deposited on PGS at sweep rates of 100 mV/s, 200 mV/s, and 300 mV/s. The third CV measured at each sweep rate was used to establish the capacity vs. sweep rate data in Figure 2b. Using these thickness values and assuming a density of 1.5 g/cm^3 for the pPy, 59,60 we calculate a charge capacity of 282 mAh/g (68% of pPy's theoretical capacity) at a sweep rate of 10 mV/s ($\sim 145 \text{ s}$ charge time), and a charge capacity of 211 mAh/g (50% of pPy's theoretical capacity) at a charge rate of 500 mV/s (2.9 s charge time). Furthermore, increasing the charge rate by $50\times$ from 10 mV/s to 500 mV/s only led to a 25% reduction in charge capacity. A log-log analysis of current vs. sweep rate 61 for the data in Figure 2b (not shown) identifies that the charge storage for these 5.5 nm pPy films is comprised of 15% diffusive and 85% capacitive behavior – indicating rapid charging of these thin redoxactive layers. We note that the double layer capacity of bare PGS substrates corresponded to only 10% of the total capacity at 10 mV/s sweep rate and 5% of the total capacity at a 500 mV/s sweep rate – a small fraction of the capacitive charge storage from the log-log analysis.

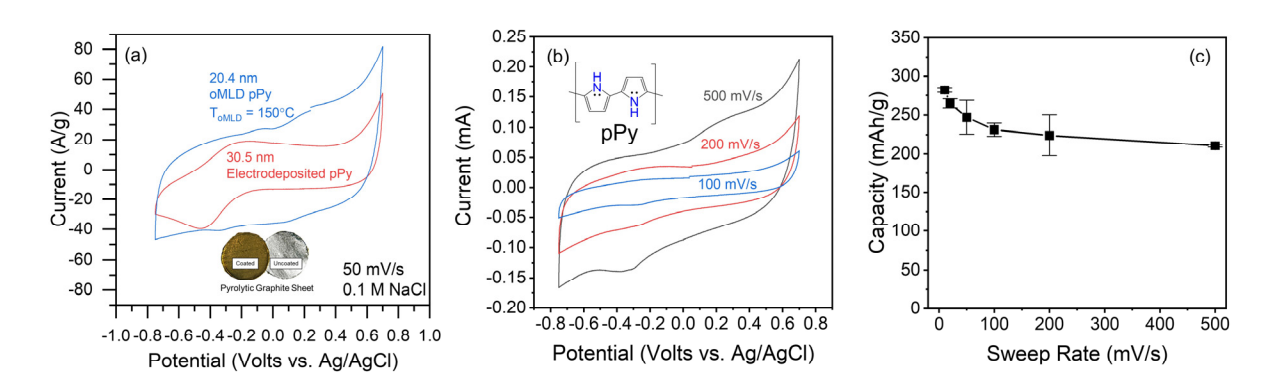


Figure 2. Electrochemical properties of pPy films formed by oMLD on PGS at 150 °C including (a) comparison of CV of 20.4 nm thick oMLD pPy vs. 30.5 nm electrodeposited pPy, (b) comparison of CV of 5.5 nm thick oMLD pPy films at varying sweep rates and (c) corresponding charge capacities from the third CV cycle of (b) for triplicate samples with sweep rates in randomized order between samples. The inset on the bottom of (a) shows PGS before and after Py/MoCl₅ oMLD with a visible change in color from the deposited film.

We emphasize that based on the above analysis, the electrochemical capacities for thin-film oMLD pPy are initially as high as 282 mAh/g. This is approximately two times higher than typical values of the electrochemical capacity reported for pPy formed by other synthesis methods. For reference, assuming every nitrogen atom yields one stoichiometric electron transfer, the maximum theoretical specific capacity for pPy is 412 mAh/g. However, typical values of charge storage capacity for pPy are ~140 mAh/g, corresponding to ~1/3 of the theoretical capacity. The highest capacity value reported for electrodeposited pPy is 133 mAh/g (480 F/g over 1.0 V potential window) at a sweep rate of 10 mV/s, and the highest value from chemical oxidative formation of pPy is 111 mAh/g (500 F/g over a 0.8 V potential window) at a sweep rate of 2 mV/s. These values are consistent with the capacity of 128.4 mAh/g we measure on a 30.5 nm thick electrodeposited pPy in Figure 2a.

The practical capacity limit for pPy of 140 mAh/g has been is thought to originate from irreversible formation of electrically resistive and nonideal polymer structures ^{17–19} arising from uncontrolled polymer formation, limiting the activity to ~1/3 of amine groups within pPy.⁴ We attribute the two-fold enhancement in electrochemical capacity we observe here to three factors: (1) controlled oMLD surface reactions generating favorable local polymer structures for redox reactivity, (2) incorporation of MoCl_x into the polymer structure to prevent pore collapse of the pPy, and (3) reduction in the length scale for ion and electron transport enabled by thin film growth. Previous VPP deposition studies have only achieved capacities of 118 mAh/g for pPy by oCVD³⁸ and 29 mAh/g for pAni by oCVD.⁷² However, as described in the introduction, oCVD proceeds via homogenous reactions like electrodeposition and chemical oxidation, and is therefore expected to produce similar molecular structures (and electrochemical capacities) to pPy formed by electrodeposition and chemical oxidation.

We note that within 50 CV cycles, the capacity of each of the oMLD pPy films decreases and stabilizes at values of <140 mAh/g (*vide infra*). This capacity decrease gives rise to the breaks in the CV data in Figure 2a and 2b corresponding to the start/end of the CV cycle at the open circuit voltage (~0.1 V vs. Ag/AgCl). Similar breaks are observed in below CV data for the same reason. Nonetheless, the high initial capacity values reported in Figure 2 show promise for further refinement to employ ultra-thin oMLD pPy films to produce high-rate electrochemical devices.

Mechanistic Insights from oMLD of Ani and PDA oMLD of Ani and PDA

After establishing oMLD chemistry for Py/MoCl₅, we were interested to form pAni thin films by oMLD using sequential doses of Ani and MoCl₅ to identify whether oMLD also enhances the electrochemical capacity of pAni. Similar to pPy, the electrochemical capacity of pAni has been limited to ~1/2 of its maximum theoretical capacity using conventional deposition approaches.4 However, the oMLD growth behavior of pAni resulted in unexpected growth behavior, as described in SI Section B, indicating a different oMLD growth process that is not consistent with pPy oMLD above, or previous reports of oMLD of pEDOT. While Py/MoCl₅ produced redox activity in line with our expectations for the formation of pPy, the Ani/MoCl₅ films did not exhibit the expected electrochemical activity for pAni in aqueous electrolyte regardless of the growth temperature or thickness employed. For example, the CV data for a 83 nm thick Ani/MoCl₅ film deposited at via 300 oMLD cycles at 150 °C is shown in Figure 3 compared with a typical response for an oMLD pPy film (data for 7.7 nm thick pPy film shown). This Ani/MoCl₅ oMLD film exhibited a specific capacitance of 58.8 mAh/g – only 20% of the maximum theoretical capacity of pAni, and well below specific capacities of 150 mAh/g reported for pAni formed by established deposition techniques.⁴ The Ani/oMLD film also does not exhibit sharp redox features at 0.13 V and 0.41 V vs. Ag/AgCl, as would be expected for pAni at the pH of 3.5 employed in these experiments.^{31,73} This suggests that the Ani/MoCl₅ oMLD process does not yield pAni films. This is surprising, as oMLD is thought to proceed via oxidation and quenching of surface monomers, which should be equally viable for Ani and Py. This result suggests that previous descriptions of the oMLD mechanism are incomplete.

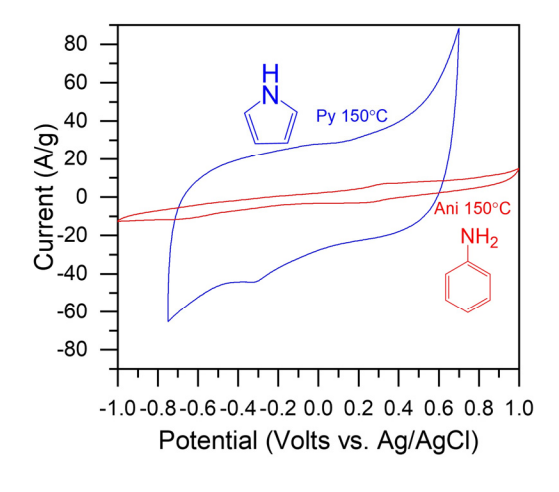


Figure 3. Comparison between electrochemical CV reponse of Py/MoCl₅ vs. Ani/MoCl₅ oMLD films deposited at 150 °C.

Considering the difference in growth behavior and electrochemical properties between Ani and Py oMLD films, we hypothesized that the local geometry of the monomer influences the reaction pathway for polymerization by oMLD. Specifically, considering that oMLD proceeds via self-limiting surface reactions, we propose that MoCl₅ binds to surface amine groups and forms an –R-NH_x-MoCl₅ surface adduct,^{74–76} and that this surface adduct drives polymerization at sites adjacent to the amine, near the MoCl₅ surface species. For the Py monomer, the favorable sites for polymerization are at the alpha carbons adjacent to the amine, and an MoCl₅ surface adduct is expected to allow coordination of two monomers on the surface to facilitate this polymerization, as depicted in Figure 4a. This mechanism would also apply to oMLD of EDOT, which has a 5-membered heterocycle structure similar to Py. In contrast, the favorable polymerization site for the Ani monomer in solution-phase reactions is at the para position on the benzene ring opposite the amine, but when two Ani molecules coordinate with one MoCl₅ in a surface adduct, reaction at this para position is not viable, as depicted in Figure 4b.

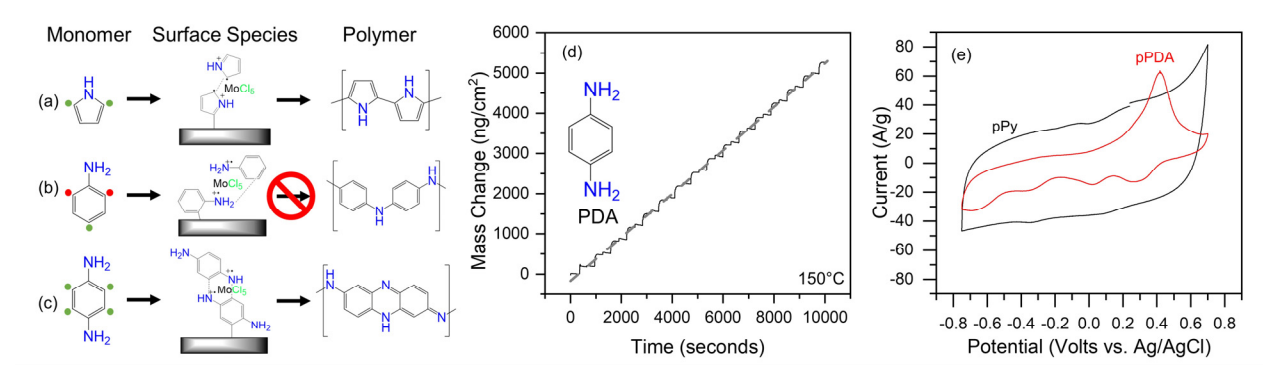


Figure 4. Proposed surface species of MoCl₅ coordinating with (a) Py, (b) Ani, (c) PDA identifying that Py and PDA commonly react adjacent to the amine but Ani does not. This concept is consistent with (d) QCM growth study of pPDA at 150 °C showing facile nucleation and growth of pPDA by oMLD and (e) CV of oMLD pPDA film showing redox activity. The dashed line in (d) represents a linear fit of the QCM data. CVs in (e) were performed at 50 mV/s in 0.1 M NaCl electrolyte.

Based on this picture of how MoCl₅ is expected to coordinate with Py and Ani surface monomers in Figure 4a and 4b, we hypothesized that the PDA monomer would exhibit oMLD

growth with MoCl₅ to yield redox-active poly-PDA (pPDA) films as depicted in Figure 4c. The PDA monomer is a derivative of Ani with a second amine group in the para position. The presence of this second amine group in the para position drives favorable polymerization at the four free carbons on the benzene ring highlighted in green in Figure 4c to form phenazine moieties as depicted in Figure 4c.⁷⁷ The reaction at these sites is also viable based on the surface coordination with MoCl₅. In Figure 4d, we depict QCM data of the steady-state oMLD growth of PDA/MoCl₅ at 150 °C. We observe saturating dose behavior for both precursor exposures, and linear growth with an MGPC of 251 ng/cm². In Figure 4e we depict CV measurements in aqueous electrolyte for a pPDA film grown by oMLD. We observe four distinct redox features for the pPDA oMLD film on a reducing sweep from +0.70 to -0.75 V vs. Ag/AgCl, consistent with a blend of primary amines and phenazine groups within pPDA. 78-80 This result confirms that oMLD using the PDA monomer is viable for producing redox-active films and supports our hypothesis that the MoCl₅ adduct drives polymerization at sites adjacent to the amine. However, interestingly, the capacity we measure for the pPDA oMLD film is 128 mAh/g, only ~25% of its maximum theoretical capacity of 500 mAh/g (assuming two redox-active amines per monomer). In contrast, the oMLD pPy film in Figure 4e achieved 63% of the maximum theoretical capacity of pPy. Although more distinct redox activity is observed for oMLD of pPDA relative to pAni, the redox capacity relative to the theoretical capacity is not significantly enhanced for pPDA relative to pAni oMLD.

Based on the surface coordination and reaction picture in Figure 4a-c, we hypothesized that the lower electrochemical capacity for pAni and pPDA films may arise because primary amine (R-NH₂) groups in Ani and PDA may also react to form azo (R-N=N-R) groups. To examine this, we performed Raman spectroscopy on both Py/MoCl₅ and Ani/MoCl₅ oMLD films as depicted in Figure 5a-c and compared these against reference spectra for pPy and pAni. The Raman peaks for the Py/MoCl₅ oMLD film are all consistent with the peaks expected for pPy as depicted in Figure 4a.^{81,82} Although Ani/MoCl₅ oMLD Raman measurements reveal characteristic peaks for pAni in Figure 5b,⁸³ we also observe a clear peak at 1480 cm⁻¹ in the Ani/MoCl₅ Raman spectrum that is consistent with the azo (R-N=N-R) group in azobenzene.^{84,85} Unfortunately, the remainder of the Raman peaks for azobenzene overlap with peaks expected for pAni, except for strong peaks at 1575 and 1580 cm⁻¹,^{85,86} and these two peaks overlap with a peak from the PGS substrate employed in Figure 5b. To confirm the presence of azobenzene, we performed Raman spectroscopy on an Ani/MoCl₅ oMLD film deposited on an anodic aluminum oxide (AAO) substrate in Figure 5c,

where the AAO substrate does not interfere with peaks at 1575 and 1580 cm⁻¹. Here, we observe clear features at 1575 and 1580 cm⁻¹ for the Ani/MoCl₅ oMLD film deposited on the AAO substrate and features consistent with all the dominant peaks in azobenzene, confirming that Ani/MoCl₅ oMLD produces azobenzene. The oxidative formation of azo groups from primary amines has been described in prior work,⁸⁷ and recent reports have shown formation of azobenzene by oxidation of aniline on Mo-based catalysts.⁸⁸ However, to our knowledge this is the first report of the formation of an azopolymer using a VPP process.

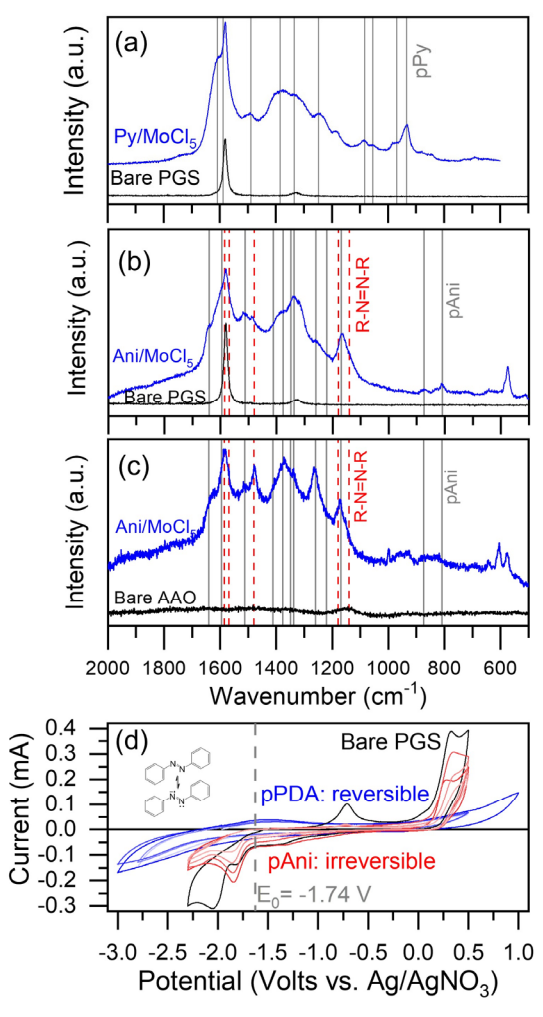


Figure 5. Raman spectroscopy results for (a) Py/MoCl₅ oMLD film on PGS, (b) Ani/MoCl₅ oMLD film on PGS, (c) Ani/MoCl₅ oMLD film on AAO. Also shown are (d) CV experiments in nonaqueous acetonitrile electrolyte at a sweep rate of 50 mV/s for a 121 nm Ani/MoCl₅ oMLD film on PGS (red), a 40.3 nm PDA/MoCl₅ oMLD film on PGS (blue), and bare PGS substrate (black).

The formation of azo groups by oMLD surface reactions demonstrated here provides a route to grow thin-film azo-polymers, where the growth conditions may be adjusted to be selective for azo formation to produce, e.g. polyazobenzene homopolymer. Just as the primary amines in Ani react during Ani/MoCl₅ oMLD to produce azobenzene, we expected that the primary amines in PDA will also react with MoCl₅ to form azo groups within pPDA -forming polyazobenzenedomains. 87 The formation of thin-film polyazobenzene could be valuable for use in anode materials in alkali-ion (e.g. Li-ion) batteries due to the highly anodic (negative) redox potential of azo groups. 85 Azobenzene-containing polymers are also of interest for their opto-mechanical properties.⁸⁹ To identify whether azo groups were formed during PDA/MoCl₅ oMLD, we performed nonaqueous electrochemical measurements on PGS substrates subjected to Ani/MoCl₅ and PDA/MoCl₅ oMLD processes as depicted in Figure 5d to look for electrochemical signatures consistent with azo groups. We find that both Ani/MoCl₅ and PDA/MoCl₅ oMLD films exhibit electrochemical reduction at -1.74 V vs. Ag/AgNO₃, consistent with reduction of azo groups to form azo anion radicals. 90,91 This redox process is reversible in pPDA films with a capacity of 185 mAh/g measured on the oxidizing sweep (vs. 500 mAh/g max theoretical), and initial cycling results up to 10 CV cycles suggest that the azo groups are stable in the condensed phase formed by PDA/MoCl₅ oMLD.

We note that the electrochemical redox process at -1.74 V vs. Ag/AgNO₃ is irreversible for Ani/MoCl₅ oMLD films and decreases with repeated cycling. We attribute this decrease to the dissolution of azobenzene molecules upon electrochemical reduction to form azobenzene anion radicals. Because each Ani monomer has only one amine group, the reaction of two Ani molecules is expected to form azobenzene or short-chain azo oligomers that easily dissolve in nonaqueous electrolyte when charged. This was confirmed by UV-Vis spectroscopy (not shown) of the electrolyte after CV cycling of the Ani/MoCl₅ oMLD films in acetonitrile, which showed an absorption peak at 300 – 350 nm, consistent with the presence of azobenzene.⁹² We also observed visible loss of the deposited Ani/MoCl₅ layer from PGS following electrochemical cycling for the area of the PGS sample exposed to the electrolyte. We note that the presence of redox activity in pPDA films under more positive potentials (-0.75 – 0.75 V vs. Ag/AgCl) in Figure 4e suggests that not all amine R-NH₂ groups on PDA have reacted to form azo (R-N=N-R) groups during PDA/MoCl₅ oMLD, instead producing a blend of both azo moieties (depicted in the inset of Figure 5d), and phenazine-like moieties (depicted as the product in Figure 4c). Based on the measured

electrochemical capacities corresponding to phenazine (Figure 4e – 128 mAh/g) and azo (Figure 5d – 185 mAh/g) moieties, we expect that these groups exist in a ~2:3 phenazine:azo molar ratio within PDA/MoCl₅ oMLD films deposited in this work. We expect that oMLD growth conditions (e.g. growth temperature and dosing scheme) can be tuned in future work to control the phenazine vs. azo character, and generate polyazobenzene homopolymers.

Controlling Polymer Structure from oMLD of Molecularly Assembled Py/PDA Copolymers

Based on the above understanding of the oMLD mechanism, we expected that introducing Py monomers during PDA/MoCl₅ oMLD growth would block azo-formation and direct PDA to react to form phenazine-like moieties, yielding higher electrochemical capacities under cathodic potentials. In SI Section C, we examine the growth rate and uniformity of molecularly assembled copolymers of Py and PDA and identify rapid nucleation and growth and facile surface coreactions of the PDA and Py monomers. We then employed CV measurements to identify how assembling these monomers into controlled copolymers impacted the redox features for azo, phenazine, and Py moieities. In Figure 6a-c, we depict aqueous CV experiments of oMLD films grown using 1:1, 5:1, and 20:1 cycle ratios of Py:PDA oMLD cycles. If the monomers were to form discrete pPDA and pPy domains, we would expect that the redox activity for the oMLD copolymers would appear as a superposition of pPy and pPDA electrochemical responses. Instead, we observe a response where the qualitative shape of the CV changes depending on the Py:PDA cycle ratio in Figure 6a-c. This indicates that by alternating doses of the Py and PDA monomers during oMLD growth in different ratios, we control the assembly of these monomers to form qualitatively different local molecular structures with different electrochemical properties. For the 1:1 Py:PDA cycle ratio, we observe a CV in Figure 6a that is similar to PDA-only oMLD films, but with enhanced redox-activity on the oxidizing sweep at +0.6 V and on the reducing sweep at -0.7 V vs. Ag/AgCl relative to PDA-only oMLD. Although the redox potential of each monomer may be expected to shift based on blending of molecular orbitals from these monomers within the copolymer structure, it appears that at this 1:1 cycle ratio, the redox potentials of pPDA are unshifted, and the electrochemical activity from pPy is only observed after fully oxidizing or reducing the pPDA component of the film. We note that this hysteresis effect for charge transfer observed for the 1:1 cycle ratio of Py:PDA in Figure 6a may be of interest for neuromorphic computing elements, ^{93,94} and other electronics applications (e.g. diodes). ⁹⁵

We attribute this hysteresis effect to branching effects from assembling the two monomers into a copolymer. For this 1:1 cycle ratio, the fraction of pPy in the film is expected to be small – the growth rate of pPy oMLD at 150 °C is only 0.09 nm/cycle, corresponding to ~0.23 monolayers of pPy, whereas the growth rate of pPDA oMLD at 150 °C is 1.35 nm/cycle, corresponding to ~2.4 monolayers of pPDA. Based on the relative growth rates for the two monomers, we expect that the polymer films for the 1:1 cycle ratio contain ~90% PDA monomers and ~10% Py monomers. At this low molar ratio of Py, we expect that Py monomers react on PDA in the most favorable ortho position as depicted in Figure 6d such that electrons initially flow in/out of the connected pPDA network, and only transfer to branching Py monomers after oxidizing/reducing the PDA molecular constituents, giving rise to the irreversible electrochemical behavior observed for the 1:1 Py:PDA cycle ratio in Figure 6a.

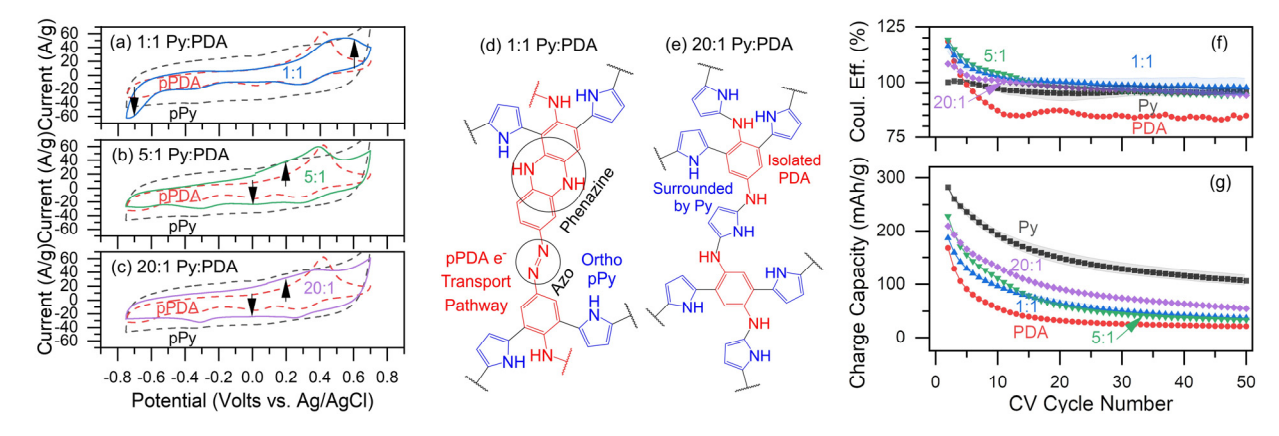


Figure 6. Comparison of cyclic voltammograms of pPy (20.4 nm thickness), pPDA (40.3 nm thickness) against (a) 1:1 pPy:pPDA copolymer (48.5 nm thickness), (b) 5:1 pPy:pPDA copolymer (49.7 nm thickness) and (c) 20:1 pPy:pPDA copolymer (29.5 nm thickness) at a sweep rate of 50 mV/s in aqueous electrolyte tuned to a pH of 3.5. A low Py content for the 1:1 cycle ratio drives irreversible charge storage, which we attribute to Py branching from pPDA domains as depicted in (d), whereas a high Py content leads to more reversible charge storage for the Py constituent which we attribute to isolated PDA monomers surrounded by PDA as depicted in (e). This interpretation is corroborated by the (f) coulombic efficiency and (g) specific capacity during extended cycling. The shaded areas around each data set in (f) and (g) represent the standard deviation from replicate measurements.

To confirm this interpretation, we increased the cycle ratio of Py:PDA from 1:1 to 5:1 and 20:1. The film thicknesses for the data reported in Figure 6 were 20.4, 40.3, 48.5, 49.7, and 29.5 nm for Py, PDA, and 1:1, 5:1, 20:1 Py/PDA copolymer films, after 150, 30, 30, 150, and 210 total oMLD cycles (sum of Py/MoCl₅ and PDA/MoCl₅ cycles), respectively. Based on the growth rates of the independent Py/MoCl₅ and PDA/MoCl₅ oMLD chemistries, the 5:1 and 20:1 cycle ratios correspond to ~1:2 and ~2:1 molar ratios of Py:PDA monomers, respectively, within the molecularly assembled copolymer films. In Figure 6b,c, we see that as the ratio of Py:PDA oMLD cycles increases above 1:1 to 5:1 and 20:1, the redox process arising from the pPy constituent of the film ($E_0 = -0.2 \text{ V}$ vs. Ag/AgCl) becomes more reversible. On the oxidizing sweep, the additional charge storage capacity provided from introducing Py into pPDA shifts from a redox potential of 0.6 V at a 1:1 cycle ratio (higher potential than the oxidation peak for pPDA) to a potential of 0.2 V for the 5:1 and 20:1 cycle ratio (lower potential than the oxidation peak for pPDA). Likewise, on the reducing sweep, as the amount of Py within the film increases, the amount of cathodic current at a potential of -0.7 V decreases, and the amount of anodic current between +0.3 and -0.5 increases – as highlighted with arrows in Figure 6a-c. Under the 20:1 cycle ratio condition, we expect that Py monomers more completely surround PDA monomers within the copolymer film, as depicted in Figure 6e. The 5:1 and 20:1 cycle ratios (with ~1:2 and ~2:1 molar ratios of each monomer based on the QCM growth rates of each isolated monomer) exhibit qualitatively different redox features from either the PDA-only or Py-only polymers, indicating that molecular assembly of these monomers into intimate copolymers causes different reactions and/or molecular orbital mixing for adjacent monomers, impacting the equilibrium redox potentials we observe. By adjusting the cycle ratio of the two monomers, we achieve different molecular structure and monomer interaction effects, yielding different redox properties for each copolymer composition.

The interpretation of differences in molecular branching character depending on the Py content in the Py:PDA copolymers depicted in Figure 6d and 6e is corroborated by the coulombic efficiency and stability of the films in Figure 6f and 6g. Phenazine moieties are susceptible to oxidative decomposition and disproportionation in the presence of hydroxyls, 80 leading to a low coulombic efficiency in Figure 6f and rapid decay in electrochemical capacity vs. cycle number in Figure 6g for pure PDA/MoCl₅ oMLD films. By introducing just ~10 mol% Py into the pPDA film using a 1:1 Py:PDA cycle ratio, the coulombic efficiency increases from ~80% to >95% and the

electrochemical cycling stability improves relative to pure pPDA. We attribute this to branching Py monomers that interconnect pPDA domains and prevent oxidative decomposition. This improvement in coulombic efficiency is also observed for the 5:1 and 20:1 cycle ratios. The 5:1 and 20:1 cycle ratios would be expected to result in the highest electrochemical capacity in aqueous electrolyte by disrupting azo formation, but we expect that the hydrophilic nature of the resulting branched structure depicted schematically in Figure 6e may facilitate dissolution in the aqueous electrolyte employed in Figure 6, giving rise to the lower capacity and more rapid capacity loss for these cycle ratios in Figure 6g. We note that the capacity loss we observe for all the compositions in Figure 6g is common for redox-active polymers and is typically attributed to densification and/or chemical decomposition. The capacity loss may be addressed in future work by adjusting the potential window, 32,98,99 introducing monomer substituents, and/or modifying the polymer surface.

To further confirm our understanding of how altering the Py:PDA cycle ratio impacts the molecular structure within the polymer films, we performed nonaqueous CV measurements on pure PDA/MoCl₅ oMLD films (0:1 Py:PDA cycle ratio) and the 1:1 and 5:1 cycle ratio copolymers as depicted in Figure 7. In these measurements, we observe that as we increase the number of Py cycles, we observe a decrease in the redox activity in the potential window for azo formation (i.e. more reducing potentials of 1.7 to 0.9 V vs. Na/Na⁺ in Figure 7). We find that the specific capacity on the cathodic sweep from 1.7 to 0.9 V vs. Na/Na⁺ arising from azo functionality is 204 mAh/g, 134 mAh/g, and 137 mAh/g for the 0:1, 1:1, and 5:1 Py:PDA cycle ratios, respectively, This confirms that increasing the amount of Py oMLD cycles disrupts formation of azo groups within the copolymer films as we depict in Figure 6e. Likewise, as the number of Py cycles increases from a 0:1 to 5:1 Py:PDA ratio, we observe an increase in the redox activity at more oxidizing potentials of 1.5 to 3.3 V vs. Na/Na⁺, which corresponds to the potential window for phenazine and pPy functionality. The specific capacity on the cathodic sweep from 3.3 to 1.5 V in Figure 7 arising from pPy/phenazine character is 95 mAh/g, 101 mAh/g, and 292 mAh/g for the 0:1, 1:1, and 5:1 cycle ratios, respectively. We note that this potential window of 3.3 – 1.5 V vs. Na/Na⁺ on the cathodic sweep was selected for this analysis to not include the irreversible peak observed at more oxidizing potentials for the 5:1 Py:PDA cycle ratio. We also note that the 20:1 cycle ratio sample was not included in this analysis because irreversible peaks under both reducing (+1.0 V vs. Na/Na⁺) and oxidizing (+3.5 V vs. Na/Na⁺) potentials dominated the electrochemical behavior for this cycle ratio. We observed similar irreversible response for pure pPy films in nonaqueous electrolyte. The origins of the irreversible processes in nonaqueous electrolyte for the Py-rich films may arise from catalytic decomposition of the electrolyte or from dissolution/decomposition of the polymer films, but this is unclear with the present data. Overall, these nonaqueous electrochemical results support that oMLD provides control over the molecular composition of polymer films using different oMLD cycle ratios outlined in Figure 6d and 6e. We emphasize that controlled molecular assembly of copolymers is not possible by conventional oCVD and other VPP processes, and this work represents the first demonstration of this concept.

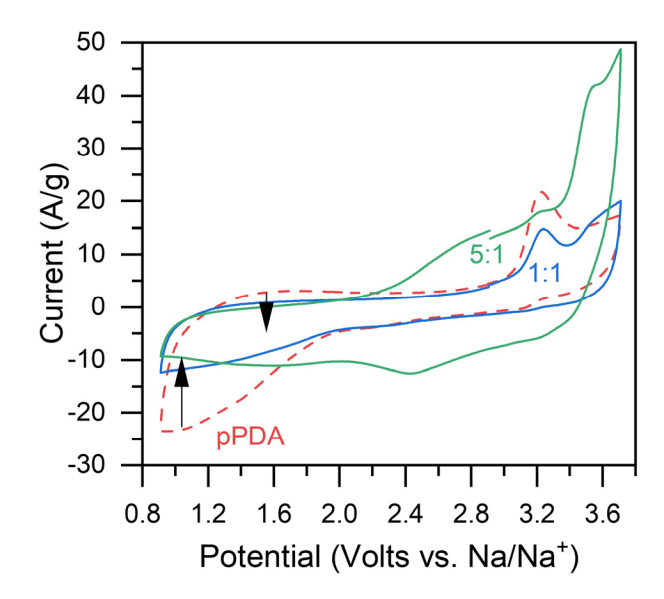


Figure 7. Nonaqueous cyclic voltammetry at a sweep rate of 20 mV/s in 0.1 M NaClO₄ in acetonitrile for 40.3 nm thick pPDA (dashed red), 48.5 nm thick 1:1 Py:PDA cycle ratio (blue) and 49.7 nm thick 5:1 Py:PDA cycle ratio (green) films grown by oMLD on PGS substrates.

Conclusion

In this work, we report the first demonstration of oMLD of amine-containing conjugated polymers that are lower cost and exhibit higher electrochemical capacity than previously reported pEDOT oMLD films. We find that oMLD of amine-containing monomers proceeds via irreversible chemisorption of each precursor to produce redox-active films with molecular-scale thickness control. This oMLD approach allows for the formation of conformal and uniform films of pPy on 3D substrates, as demonstrated by uniform coating into porous channels to an aspect

ratio of 200:1. The ability to form conjugated amine polymers by oMLD provides a route to deliver thin films of redox-active polymers onto 3D electrode surfaces. We also identify that thin-film oMLD pPy exhibits capacities up to 282 mAh/g - 68% of pPy's theoretical capacity, and maintains 50% of the theoretical capacity of pPy when charging in under 3 s. These specific capacities are up to two times higher than values of ~140 mAh/g observed for pPy synthesized by other methods,⁴ which we attribute to a favorable molecular structure for high redox activity and ultrathin ($\leq 20 \text{ nm}$) film thicknesses obtained using oMLD.

Previous work has reported similar improvements when forming thin films of inorganic redoxactive layers by ALD, where the reduction in length-scale for solid-state diffusion yields high rate charge storage for energy storage and desalination applications. However, the barrier preventing the adoption of ALD coatings has been the high-cost organometallic precursors needed to form inorganic active layers by ALD. Here, we demonstrate the formation of redox-active polymer layers with high electrochemical capacities 12,73 using low-cost organic precursors comprised of earth-abundant elements. This provides a more economically viable and sustainable route for the use of an ALD-like process (here, oMLD) to deliver high-performance materials in a thin-film geometry for redox-active electrodes. In particular, the high capacity of pPy films in aqueous electrolytes makes them of interest as electrode materials (1) for aqueous batteries, (2) as supercapacitor electrodes, and/or (3) as ion-uptake uptake in electrochemical desalination.

We also identify that while oMLD of Py/MoCl₅ produces pPy films, oMLD of Ani/MoCl₅ and PDA/MoCl₅ chemistries produce azo groups (azobenzene and polyazobenzene, respectively). We attribute this to the coordination of the MoCl₅ oxidant to nucleophilic amine groups on the growth surface, driving reactions adjacent to the amine, and leading to the formation of azo groups for primary amines. This provides an improved picture of the oMLD mechanism over previous reports, identifying that the surface coordination geometry is important to understand oMLD growth processes. This result also opens avenues to harness this mechanistic understanding to direct surface polymerization and control the molecular structure of conjugated polymer films using oMLD. The azo-polymer films produced by PDA/MoCl₅ oMLD exhibit redox activity at -1.7 V vs. Ag/AgNO₃ (+1.5 V vs. Na/Na⁺) in nonaqueous electrolyte. This reversible redox activity at highly anodic (negative) potentials through electrochemical reduction of azo groups makes these PDA/MoCl₅ oMLD films of interest as anode materials for alkali ion batteries.⁸⁵

Finally, we report the molecular assembly of Py and PDA monomers by alternating between oMLD cycles of Py/MoCl₅ and PDA/MoCl₅ chemistries during oMLD growth. These molecularly assembled copolymer Py/PDA oMLD films exhibit qualitatively different electrochemical behavior from the films formed using the isolated constituent monomers. We demonstrate control over molecular constituents within the film by alternating the ratio of oMLD cycles of each monomer, yielding different electrochemical responses. The controlled molecular assembly of copolymers we demonstrate here using sequential surface reactions via oMLD provides a route to achieve pristine control over the molecular structure of conjugated polymers and will allow us to examine how molecular structure impacts electrical and electrochemical properties in future work. This is of particular interest considering recent work establishing understanding of the semi-localized charge transport in conducting polymers, ¹⁰⁴ where control over monomer ordering in polymer chains will allow us to examine the molecular origins of charge transport physics in conjugated polymers.

Materials and Methods

Oxidative Molecular Layer Deposition

oMLD in this work was carried out using a hot walled ALD-type reactor, ¹⁰⁵ utilizing sequentially dosed chemical precursors separated by argon carrier gas at reduced pressures (~0.8 Torr). The deposition temperature of the main reaction chamber was held at temperatures between 100 °C and 200 °C using PID temperature controllers. Py (98%, Fischer Scientific) was held at room temp, while Ani (99.9%, Fischer Scientific), PDA (97+%, Fischer Scientific), and MoCls (99.6%, Fischer Scientific) were held at 80 °C, each in a jacketed flow-over precursor bubbler with PID temperature control. The peak dose pressures of Py, Ani, PDA, and MoCl₅ were 100 mTorr, 15 mTorr, 10 mTorr, and <5 mTorr, respectively. 200 sccm of continuous Ar carrier gas flow was used during depositions to maintain a baseline pressure of ~0.8 Torr.

Prior to each deposition, the reactor and sample tray were passivated with at least 150 oMLD cycles of the target chemistry. Substrates used for various depositions included Si pieces (Silicon Valley Microelectronics), AAO membranes (InRedox), quartz wafers (Valley Design), and PGS (Newark). The samples were pre-heated in the reaction chamber under inert carrier gas purge for at least 30 min prior to deposition. During each oMLD growth, the monomer (A) and oxidant (B) were dosed sequentially in A/B precursor cycles, with a purge step between each

precursor dose. A typical dosing scheme for one oMLD cycle consisted of 10 s of monomer dose, 100 s of Ar purge, 100 s of MoCl₅ oxidant dose, and 100 s of purge. These cycles were repeated to increase the thickness of the resulting polymer films. Dose and purge times varied based on monomer and temperature used during deposition, as indicated in the manuscript text.

Electrochemical Characterization

Three-electrode electrochemical measurements were carried out on PGS substrates in a custom electrochemical cell. The electrochemical cell provides an o-ring seal on the sample surface to expose a defined 1.21 cm² surface area to the electrolyte solution. 0.1 M NaCl aqueous electrolyte adjusted to a pH of 3.5 was used for aqueous electrochemical experiments. The electrolyte solution was purged for at least 30 minutes prior to electrochemical measurements, and a continuous Ar purge was used in the head-space of the electrochemical cell during electrochemical measurements. A graphite rod counter electrode (99.999%, Fischer Scientific) and Ag/AgCl reference electrode were used. CV experiments were performed at a sweep rate of 50 mV/s over a potential range of -0.75 to +0.75 V vs. Ag/AgCl unless otherwise noted.

Non-aqueous electrochemical experiments were performed under inert argon atmosphere (<0.5 ppm H₂O, <0.3 ppm O₂) in a glovebox. A 0.1 M NaClO₄ in anhydrous, amine free acetonitrile (Alfa Aesar, 99.9%) was employed as an electrolyte. A custom glass three-electrode cell was used for electrochemical experiments with a graphite rod as the counter electrode (99.5%) and a non-aqueous Ag/AgNO₃ reference electrode (BASi). CV experiments were performed at a scan rate of 20 mV/s within a voltage window no greater than -3.0 V and 1.0 V vs Ag/AgNO₃. The Ag/AgNO₃ reference potential was calibrated using ferrocene to report potentials vs. Na/Na⁺.

The specific capacity, C_C , and specific capacitance, C_F , of films reported in the text were calculated as $C_C = \frac{\Delta Q}{\rho Ah}$ and $C_F = \frac{\Delta Q}{\Delta V \rho Ah}$, where ΔQ is the total charge transferred on the charging sweep (cathodic sweep for aqueous electrolyte, and as-specified above for nonaqueous experiments), ΔV is the potential window (1.45 V, -0.75 to +0.70 V vs. Ag/AgCl for aqueous electrolyte, and as-specified above for nonaqueous experiments), ρ is the density of the film (taken as 1.5 g/cm³ for pPy ^{58,59} and 1.1 g/cm³ for pPDA based on typical pAni densities, ^{106,107} and 1.3 g/cm³ for the molecularly assembled copolymers), A is the cross-sectional area of film exposed to

the electrolyte (1.27 cm²), and h is the film thickness for each sample as measured by SE on Si witness wafers, and benchmarked using NR and SEM.

Neutron Reflectivity

NR data was obtained using the Grazing Incidence Neutron Spectrometer (GANS) at the University of Missouri Research Reactor (MURR).¹⁰⁸ Analysis was done through the Reflpak suite¹⁰⁹ which uses the Parratt method¹¹⁰ that recursively accounts for the film layers and interfaces to construct a final film density profile. The fringe spacing in the reflectivity curves is a product of the layer thickness.

Scanning Electron Microscopy

SEM was used to evaluate deposited thickness using a FEI Scios Dual Beam FIB SEM. High contrast SEM images of the deposited polymer film were visualized under 5 keV under high vacuum inert conditions. PGS and AAO samples were cleaved to visualize film thickness. The film thicknesses were measured using ImageJ.

Spectroscopic Ellipsometry

SE analysis and modeling were conducted using an Alpha SE system (J.A. Woollam) at an incident angle of 65°, at room temperature and open to the air and modeled using the CompleteEASE software package. The optical properties and thickness were modeled using a Cauchy-Urbach dispersion model¹¹¹ of the form $n(\lambda) = A + B/\lambda^2 + C/\lambda^4$ and $k(\lambda) = \alpha \exp(\beta (12400 (1/\lambda-1/\gamma)))$ where λ is the wavelength; A, B, C, α , and β are fitted constants to minimize error relative to NR measurements; and γ is the band edge wavelength, taken as 350 nm for oxidized pPy.¹¹² Fitted values for pPy at 100 °C were A= 1.678, B = 1.631 × 10⁻², C = 4.0814 × 10⁻³, α = 2.4052 × 10⁻¹, β =6.17 × 10⁻¹. Fitted values for pPy at 150 °C were A= 1.807, B = 1.297 × 10⁻¹, C = -1.506 × 10⁻², α = 5.8083 × 10⁻¹, β =2.618.

Raman Spectroscopy

Raman spectroscopy was conducted with a Renishaw inVia Raman spectrometer using excitation from a 633 nm laser and Raman spectra were collected over 500 – 2000 cm⁻¹ with a spectral resolution of 10 cm⁻¹. Spectra were acquired using a sweeping scan of 10 cm⁻¹/s and a laser power of 10.1 mW.

Supporting Information

- A. Effect of Purge Time on pPy oMLD Growth Uniformity
- B. Effect of Growth Temperature on oMLD of pAni and pPy
- C. Growth Rate and Uniformity of Py/PDA Molecularly Assembled Copolymers

Acknowledgements

M.J.Y. acknowledges support from faculty start-up funds provided by the University of Missouri Biomedical, Biological, and Chemical Engineering Department and Department of Chemistry, and partial support from the National Science Foundation (NSF) Division of Chemical, Bioengineering, Environmental, & Transport Systems (CBET) through Award Number 2131282. We thank Prof. Patrick Kinlen and Prof. Michael Harmata at the University of Missouri for useful discussions and advice. We thank Ryan Gettler at the University of Missouri for assistance with electrochemical characterization.

References:

- (1) Kim, J.; Kim, J. H.; Ariga, K. Redox-Active Polymers for Energy Storage Nanoarchitectonics. *Joule* **2017**, *I* (4), 739–768. https://doi.org/10.1016/j.joule.2017.08.018.
- (2) Li, Q.; Zheng, Y.; Xiao, D.; Or, T.; Gao, R.; Li, Z.; Feng, M.; Shui, L.; Zhou, G.; Wang, X.; Chen, Z. Faradaic Electrodes Open a New Era for Capacitive Deionization. *Advanced Science* **2020**, *7* (22). https://doi.org/10.1002/advs.202002213.
- (3) Barsan, M. M.; Ghica, M. E.; Brett, C. M. A. Electrochemical Sensors and Biosensors Based on Redox Polymer/Carbon Nanotube Modified Electrodes: A Review. *Analytica Chimica Acta* **2015**, *881*, 1–23. https://doi.org/10.1016/j.aca.2015.02.059.
- (4) Fong, K. D.; Wang, T.; Smoukov, S. K. Multidimensional Performance Optimization of Conducting Polymer-Based Supercapacitor Electrodes. *Sustainable Energy & Fuels* **2017**, *1* (9), 1857–1874. https://doi.org/10.1039/c7se00339k.
- (5) Machida, S.; Miyata, S.; Techagumpuch, A. Chemical Synthesis of Highly Electrically Conductive Polypyrrole. *Synthetic Metals* **1989**, *31* (3), 311–318. https://doi.org/10.1016/0379-6779(89)90798-4.
- Yoon, C. O.; Reghu, M.; Moses, D.; Heeger, A. J.; Cao, Y.; Chen, T. A.; Wu, X.; Rieke, R. D. Hopping Transport in Doped Conducting Polymers in the Insulating Regime near the Metal-Insulator Boundary: Polypyrrole, Polyaniline and Polyalkylthiophenes. Synthetic Metals 1995, 75 (3), 229–239. https://doi.org/10.1016/0379-6779(96)80013-0.

- (7) Wang, X.; Zhang, X.; Sun, L.; Lee, D.; Lee, S.; Wang, M.; Zhao, J.; Shao-Horn, Y.; Dincă, M.; Palacios, T.; Gleason, K. K. High Electrical Conductivity and Carrier Mobility in OCVD PEDOT Thin Films by Engineered Crystallization and Acid Treatment. *Science Advances* **2018**, *4* (9), 1–10. https://doi.org/10.1126/sciadv.aat5780.
- (8) Lock, J. P.; Im, S. G.; Gleason, K. K. Oxidative Chemical Vapor Deposition of Electrically Conducting Poly(3,4-Ethylenedioxythiophene) Films. *Macromolecules* **2006**, 39 (16), 5326–5329. https://doi.org/10.1021/ma0601130.
- (9) Pasta, M.; Wessells, C. D.; Cui, Y.; Mantia, F. la; la Mantia, F.; Mantia, F. la. A Desalination Battery. *Nano Lett* **2012**, *12* (2), 839–843. https://doi.org/10.1021/nl203889e.
- (10) Lee, J.; Kim, S.; Yoon, J. Rocking Chair Desalination Battery Based on Prussian Blue Electrodes. *ACS Omega* **2017**, *2* (4), 1653–1659. https://doi.org/10.1021/acsomega.6b00526.
- (11) Dühnen, S.; Nölle, R.; Wrogemann, J.; Winter, M.; Placke, T. Reversible Anion Storage in a Metal-Organic Framework for Dual-Ion Battery Systems. *J Electrochem Soc* **2019**, *166* (3), A5474–A5482. https://doi.org/10.1149/2.0681903jes.
- (12) Davis, V. K.; Bates, C. M.; Omichi, K.; Savoie, B. M.; Momčilović, N.; Xu, Q.; Wolf, W. J.; Webb, M. A.; Billings, K. J.; Chou, N. H.; Alayoglu, S.; McKenney, R. K.; Darolles, I. M.; Nair, N. G.; Hightower, A.; Rosenberg, D.; Ahmed, M.; Brooks, C. J.; Miller, T. F.; Grubbs, R. H.; Jones, S. C. Room-Temperature Cycling of Metal Fluoride Electrodes: Liquid Electrolytes for High-Energy Fluoride Ion Cells. *Science* (1979) **2018**, 362 (6419), 1144–1148. https://doi.org/10.1126/science.aat7070.
- (13) Runge, F. F. Ueber Einige Produkte Der Steinkohlendestillation. *Annalen der Physik und Chemie* **1834**, *107* (5), 65–78. https://doi.org/10.1002/andp.18341070502.
- (14) Letheby, H. On the Production of a Blue Substance by the Electrolysis of Sulphate of Aniline. *J. Chem. Soc.* **1862**, *15*, 161–163. https://doi.org/10.1039/JS8621500161.
- (15) Tian, Y.; Zeng, G.; Rutt, A.; Shi, T.; Kim, H.; Wang, J.; Koettgen, J.; Sun, Y.; Ouyang, B.; Chen, T.; Lun, Z.; Rong, Z.; Persson, K.; Ceder, G. Promises and Challenges of Next-Generation "beyond Li-Ion" Batteries for Electric Vehicles and Grid Decarbonization. *Chemical Reviews* **2021**, *121* (3), 1623–1669. https://doi.org/10.1021/acs.chemrev.0c00767.
- (16) Whittingham, M. S. Special Editorial Perspective: Beyond Li-Ion Battery Chemistry. *Chemical Reviews* **2020**, *120* (14), 6328–6330. https://doi.org/10.1021/acs.chemrev.0c00438.
- (17) Zotti, G. Doping-Level Dependence of Conductivity in Polypyrroles and Polythiophenes. *Synthetic Metals* **1998**, *97* (3), 267–272. https://doi.org/10.1016/s0379-6779(98)00144-1.

- (18) Holland, E. R.; Pomfret, S. J.; Adams, P. N.; Monkman, A. P. Conductivity Studies of Polyaniline Doped with CSA. *Journal of Physics Condensed Matter* **1996**, *8* (17), 2991–3002. https://doi.org/10.1088/0953-8984/8/17/011.
- (19) Peng, C.; Hu, D.; Chen, G. Z. Theoretical Specific Capacitance Based on Charge Storage Mechanisms of Conducting Polymers: Comment on 'Vertically Oriented Arrays of Polyaniline Nanorods and Their Super Electrochemical Properties.' *Chemical Communications* **2011**, *47* (14), 4105–4107. https://doi.org/10.1039/c1cc10675a.
- (20) Ayad, M. M.; Zaki, E. A. Quartz Crystal Microbalance and Spectroscopy Measurements for Acid Doping in Polyaniline Films. *Science and Technology of Advanced Materials* **2008**, *9* (1). https://doi.org/10.1088/1468-6996/9/1/015007.
- (21) Khatoon, A.; Khalid, M.; Mohammad, F. Preparation and Electroanalytical Characterization of Polyaniline: Polyacrylonitrile Composite Films. *Journal of Applied Polymer Science* **2008**, *108* (6), 3769–3780. https://doi.org/10.1002/app.28033.
- (22) Kanamura, K.; Kawai, Y.; Yonezawa, S.; Takehara, Z. Diffusion Behavior of Anions in Polyaniline during Electrochemical Undoping. 2. Effect of the Preparation Conditions of Polyaniline on the Diffusion Coefficient of BF4. *Journal of physical chemistry* **1994**, *98* (8), 2174–2179. https://doi.org/10.1021/j100059a034.
- (23) Wei, Y.; Tang, X.; Sun, Y.; Focke, W. W. A Study of the Mechanism of Aniline Polymerization. *Journal of Polymer Science Part A: Polymer Chemistry* **1989**, *27* (7), 2385–2396. https://doi.org/10.1002/POLA.1989.080270720.
- (24) Ciric-Marjanovic, G. Recent Advances in Polyaniline Research: Polymerization Mechanisms, Structural Aspects, Properties and Applications. *Synthetic Metals* **2013**, *177* (3), 1–47. https://doi.org/10.1016/j.synthmet.2013.06.004.
- (25) Noufi, R.; Nozik, A. J.; White, J.; Warren, L. F. Enhanced Stability of Photoelectrodes with Electrogenerated Polyaniline Films; CRC Press, 1982; Vol. 129.
- (26) Jones, R. A.; Bean, G. P. *The Chemistry of Pyrroles*, illustrate.; Academic Press, 1977.
- (27) Huang, J.; Kaner, R. B. Nanofiber Formation in the Chemical Polymerization of Aniline: A Mechanistic Study. *Angewandte Chemie International Edition* **2004**, *43* (43), 5817–5821. https://doi.org/10.1002/anie.200460616.
- (28) Zhang, X.; Manohar, S. K. Bulk Synthesis of Polypyrrole Nanofibers by a Seeding Approach. *J Am Chem Soc* **2004**, *126* (40), 12714–12715. https://doi.org/10.1021/ja046359v.
- (29) Chougule, M. A.; Pawar, S. G.; Godse, P. R.; Mulik, R. N.; Sen, S.; Patil, V. B. Synthesis and Characterization of Polypyrrole (PPy) Thin Films. *Soft Nanoscience Letters* **2011**, *01* (01), 6–10. https://doi.org/10.4236/snl.2011.11002.

- (30) Verma, D.; Dutta, V. Novel Microstructure in Spin Coated Polyaniline Thin Films. *Journal of Physics Condensed Matter* **2007**, *19* (18). https://doi.org/10.1088/0953-8984/19/18/186212.
- (31) Wyatt, Q. K.; Young, M. J. Pulsed Electrodeposition of Ultrathin Polyaniline Films and Mechanistic Understanding of Their Anion-Mediated Electrochemical Behavior. *Journal of The Electrochemical Society* **2020**, *167* (11), 110548. https://doi.org/10.1149/1945-7111/aba5d5.
- (32) Gettler, R.; Young, M. J. Multimodal Cell with Simultaneous Electrochemical Quartz Crystal Microbalance and in Operando Spectroscopic Ellipsometry to Understand Thin Film Electrochemistry. *Review of Scientific Instruments* **2021**, *92* (5). https://doi.org/10.1063/5.0035309.
- (33) Sayre, C. N.; Collard, D. M. Electrooxidative Deposition of Polypyrrole and Polyaniline on Self-Assembled Monolayer Modified Electrodes. *Langmuir* **1997**, *13* (4), 714–721. https://doi.org/10.1021/la960420v.
- (34) Madden, J. D.; Lafontaine, S. R.; Hunter, I. W. Fabrication by Electrodeposition: Building 3D Structures and Polymer Actuators. In *Proceedings of the International Symposium on Micro Machine and Human Science*; 1995; pp 77–81. https://doi.org/10.1109/mhs.1995.494221.
- (35) Mohammadi, A.; Lundström, I.; Inganäs, O.; Salaneck, W. R. Conducting Polymers Prepared by Template Polymerization: Polypyrrole. *Polymer (Guildf)* **1990**, *31* (3), 395–399. https://doi.org/10.1016/0032-3861(90)90375-9.
- (36) Bilger, D.; Homayounfar, S. Z.; Andrew, T. L. A Critical Review of Reactive Vapor Deposition for Conjugated Polymer Synthesis. *Journal of Materials Chemistry C* **2019**, 7 (24), 7159–7174. https://doi.org/10.1039/c9tc01388a.
- (37) Bhattacharyya, D.; Howden, R. M.; Borrelli, D. C.; Gleason, K. K. Vapor Phase Oxidative Synthesis of Conjugated Polymers and Applications. *Journal of Polymer Science, Part B: Polymer Physics* **2012**, *50* (19), 1329–1351. https://doi.org/10.1002/polb.23138.
- (38) Lee, J. E.; Lee, Y.; Ahn, K. J.; Huh, J.; Shim, H. W.; Sampath, G.; Im, W. bin; Huh, Y. il; Yoon, H. Role of Co-Vapors in Vapor Deposition Polymerization. *Scientific Reports* **2015**, *5*, 8420. https://doi.org/10.1038/srep08420.
- (39) Smolin, Y. Y.; Soroush, M.; Lau, K. K. S. Oxidative Chemical Vapor Deposition of Polyaniline Thin Films. *Beilstein Journal of Nanotechnology* **2017**, *8* (1), 1266–1276. https://doi.org/10.3762/bjnano.8.128.
- (40) Cheng, Y.; Khlyustova, A.; Chen, P.; Yang, R. Kinetics of All-Dry Free Radical Polymerization under Nanoconfinement. *Macromolecules* **2020**, *53* (24), 10699–10710. https://doi.org/10.1021/acs.macromol.0c01534.

- (41) Atanasov, S. E.; Losego, M. D.; Gong, B.; Sachet, E.; Maria, J. P.; Williams, P. S.; Parsons, G. N. Highly Conductive and Conformal Poly(3,4-Ethylenedioxythiophene) (PEDOT) Thin Films via Oxidative Molecular Layer Deposition. *Chemistry of Materials* **2014**, *26* (11), 3471–3478. https://doi.org/10.1021/cm500825b.
- (42) Kim, D. H.; Atanasov, S. E.; Lemaire, P.; Lee, K.; Parsons, G. N. Platinum-Free Cathode for Dye-Sensitized Solar Cells Using Poly(3,4-Ethylenedioxythiophene) (PEDOT) Formed via Oxidative Molecular Layer Deposition. ACS Applied Materials and Interfaces 2015, 7 (7), 3866–3870. https://doi.org/10.1021/am5084418.
- (43) George, S. M. Atomic Layer Deposition: An Overview. *Chem Rev* **2010**, *110* (1), 111–131. https://doi.org/10.1021/cr900056b.
- (44) Johnson, R. W.; Hultqvist, A.; Bent, S. F. A Brief Review of Atomic Layer Deposition: From Fundamentals to Applications. *Materials Today* **2014**, *17* (5), 236–246. https://doi.org/10.1016/j.mattod.2014.04.026.
- (45) Puurunen, R. L. Surface Chemistry of Atomic Layer Deposition: A Case Study for the Trimethylaluminum/Water Process. *Journal of Applied Physics* **2005**, *97* (121301), 1–52. https://doi.org/10.1063/1.1940727.
- (46) George, S. M.; Yoon, B.; Hall, R. A.; Abdulagatov, A. I.; Gibbs, Z. M.; Lee, Y.; Seghete, D.; Lee, B. H. Molecular Layer Deposition of Hybrid Organic Inorganic Films. **2012**.
- (47) Yoshimura, T.; Tatsuura, S.; Sotoyama, W. Polymer Films Formed with Monolayer Growth Steps by Molecular Layer Deposition. *Applied Physics Letters* **1991**, *59* (4), 482–484. https://doi.org/10.1063/1.105415.
- (48) Adamczyk, N. M.; Dameron, A. A.; George, S. M. Molecular Layer Deposition of Poly(p-Phenylene Terephthalamide) Films Using Terephthaloyl Chloride and p-Phenylenediamine. *Langmuir* **2008**, *24* (5), 2081–2089. https://doi.org/10.1021/la7025279.
- (49) Du, Y.; George, S. M. Molecular Layer Deposition of Nylon 66 Films Examined Using in Situ FTIR Spectroscopy. *Journal of Physical Chemistry C* **2007**, *111* (24), 8509–8517. https://doi.org/10.1021/jp067041n.
- (50) Piper, D. M.; Travis, J. J.; Young, M.; Son, S.-B. S. B.; Kim, S. C.; Oh, K. H.; George, S. M.; Ban, C.; Lee, S.-H. S. H. Reversible High-Capacity Si Nanocomposite Anodes for Lithium-Ion Batteries Enabled by Molecular Layer Deposition. *Advanced Materials* 2014, 26, 1596–1601. https://doi.org/10.1002/adma.201304714.
- (51) Yoon, B.; O'Patchen, J. L.; Seghete, D.; Cavanagh, A. S.; George, S. M. Molecular Layer Deposition of Hybrid Organic-Inorganic Polymer Films Using Diethylzinc and Ethylene Glycol. *Chemical Vapor Deposition* **2009**, *15* (4–6), 112–121. https://doi.org/10.1002/cvde.200806756.

- (52) Volk, A. A.; Kim, J.-S.; Jamir, J.; Dickey, E. C.; Parsons, G. N. Oxidative Molecular Layer Deposition of PEDOT Using Volatile Antimony(V) Chloride Oxidant. *Journal of Vacuum Science & Technology A* **2021**, *39* (3), 032413. https://doi.org/10.1116/6.0000791.
- (53) Ghafourisaleh, S.; Popov, G.; Leskelä, M.; Putkonen, M.; Ritala, M. Oxidative MLD of Conductive PEDOT Thin Films with EDOT and ReCl5as Precursors. *ACS Omega* **2021**, *6* (27), 17545–17554. https://doi.org/10.1021/acsomega.1c02029.
- (54) *Molecules*. https://materialsproject.org/molecules/detail/mol-224187 (accessed 2022-02-03).
- (55) Goddard, R.; Heinemann, O.; Krüger, C. Pyrrole and a Co-Crystal of 1H- and 2H-1,2,3-Triazole. *Acta Crystallographica Section C: Crystal Structure Communications* **1997**, *53* (12), 1846–1850. https://doi.org/10.1107/S0108270197009682.
- (56) Poodt, P.; Cameron, D. C.; Dickey, E.; George, S. M.; Kuznetsov, V.; Parsons, G. N.; Roozeboom, F.; Sundaram, G.; Vermeer, A. Spatial Atomic Layer Deposition: A Route towards Further Industrialization of Atomic Layer Deposition. *Journal of Vacuum Science* & Technology A: Vacuum, Surfaces, and Films 2012, 30 (1), 010802. https://doi.org/10.1116/1.3670745.
- (57) Weimer, A. W. Particle Atomic Layer Deposition. *Journal of Nanoparticle Research* **2019**, *21* (1), 9. https://doi.org/10.1007/s11051-018-4442-9.
- (58) Diaz, A. F.; Castillo, J. I.; Logan, J. A.; Lee, W.-Y. Electrochemistry of Conducting Polypyrrole Films. *Journal of Electroanalytical Chemistry and Interfacial Electrochemistry* **1981**, *129* (1–2), 115–132. https://doi.org/10.1016/S0022-0728(81)80008-3.
- (59) López Cascales, J. J.; Otero, T. F. Molecular Dynamic Simulation of the Hydration and Diffusion of Chloride Ions from Bulk Water to Polypyrrole Matrix. *Journal of Chemical Physics* **2004**, *120* (4), 1951–1957. https://doi.org/10.1063/1.1636453.
- (60) Young, M. J.; Schnabel, H.-D.; Holder, A. M.; George, S. M.; Musgrave, C. B. Band Diagram and Rate Analysis of Thin Film Spinel LiMn2O4 Formed by Electrochemical Conversion of ALD-Grown MnO. *Advanced Functional Materials* **2016**, *26* (43), 7895–7907. https://doi.org/10.1002/adfm.201602773.
- (61) Young, M. J.; Neuber, M.; Cavanagh, A. C.; Sun, H.; Musgrave, C. B.; George, S. M. Sodium Charge Storage in Thin Films of MnO2 Derived by Electrochemical Oxidation of MnO Atomic Layer Deposition Films, Supplementary Material. *Journal of The Electrochemical Society* 2015, 162 (14), A2753–A2761. https://doi.org/10.1149/2.0671514jes.
- (62) Wallas, J. M.; Young, M. J.; Sun, H.; George, S. M. Efficient Capacitive Deionization Using Thin Film Sodium Manganese Oxide. *Journal of The Electrochemical Society* 2018, 165 (10), A2330–A2339. https://doi.org/10.1149/2.0751810jes.

- (63) Sun, X.; Xie, M.; Wang, G.; Sun, H.; Cavanagh, A. S.; Travis, J. J.; George, S. M.; Lian, J. Atomic Layer Deposition of TiO2 on Graphene for Supercapacitors. *Journal of The Electrochemical Society* **2012**, *159* (4), A364–A369. https://doi.org/10.1149/2.025204jes.
- (64) Simon, P.; Gogotsi, Y. Materials for Electrochemical Capacitors. *Nature Materials* **2008**, 7 (11), 845–854. https://doi.org/10.1038/nmat2297.
- (65) Hall, P. J.; Mirzaeian, M.; Fletcher, S. I.; Sillars, F. B.; Rennie, A. J. R.; Shitta-Bey, Gbolahan. O.; Wilson, G.; Cruden, A.; Carter, R. Energy Storage in Electrochemical Capacitors: Designing Functional Materials to Improve Performance. *Energy & Environmental Science* **2010**, *3* (9), 1238–1251. https://doi.org/10.1039/c0ee00004c.
- (66) Gettler, R.; Young, M. J. Multimodal Cell with Simultaneous Electrochemical Quartz Crystal Microbalance and in Operando Spectroscopic Ellipsometry to Understand Thin Film Electrochemistry. *Review of Scientific Instruments* **2021**. https://doi.org/10.1063/5.0035309.
- (67) Wyatt, Q. K.; Young, M. J. Pulsed Electrodeposition of Ultrathin Polyaniline Films and Mechanistic Understanding of Their Anion-Mediated Electrochemical Behavior. *Journal* of The Electrochemical Society 2020, 167 (11), 110548. https://doi.org/10.1149/1945-7111/aba5d5.
- (68) Choi, C. S.; Tachikawa, H. Electrochemical Behavior and Characterization of Polypyrrole-Copper Phthalocyanine Tetrasulfonate Thin Film: Cyclic Voltammetry and in Situ Raman Spectroscopic Investigation. *J Am Chem Soc* **1990**, *112* (5), 1757–1768. https://doi.org/10.1021/ja00161a017.
- (69) Rajagopalan, B.; Kim, B.; Hur, S. H.; Yoo, I. K.; Chung, J. S. Redox Synthesis of Poly (p–Phenylenediamine)–Reduced Graphene Oxide for the Improvement of Electrochemical Performance of Lithium Titanate in Lithium–Ion Battery Anode. *Journal of Alloys and Compounds* **2017**, 709, 248–259. https://doi.org/10.1016/J.JALLCOM.2017.03.166.
- (70) Fan, L. Z.; Maier, J. High-Performance Polypyrrole Electrode Materials for Redox Supercapacitors. *Electrochemistry Communications* **2006**, *8* (6), 937–940. https://doi.org/10.1016/j.elecom.2006.03.035.
- (71) Khomenko, V.; Frackowiak, E. Determination of the Specific Capacitance of Conducting Polymer / Nanotubes Composite Electrodes Using Different Cell Configurations. **2005**, 50, 2499–2506. https://doi.org/10.1016/j.electacta.2004.10.078.
- (72) Li, X.; Rafie, A.; Smolin, Y. Y.; Simotwo, S.; Kalra, V.; Lau, K. K. S. Engineering Conformal Nanoporous Polyaniline via Oxidative Chemical Vapor Deposition and Its Potential Application in Supercapacitors. *Chemical Engineering Science* **2019**, *194*, 156–164. https://doi.org/10.1016/j.ces.2018.06.053.
- (73) Prakash, R. Electrochemistry of Polyaniline: Study of the PH Effect and Electrochromism. *Journal of Applied Polymer Science* **2002**, *83* (2), 378–385. https://doi.org/10.1002/app.10025.

- (74) Bartalucci, N.; Bortoluzzi, M.; Marchetti, F.; Pampaloni, G.; Schoch, S.; Zacchini, S. Unusual Activation Pathways of Amines in the Reactions with Molybdenum Pentachloride. *New Journal of Chemistry* **2017**, *41* (11), 4329–4340. https://doi.org/10.1039/C6NJ03992H.
- (75) Hayatifar, M.; Marchetti, F.; Pampaloni, G.; Pinzino, C.; Zacchini, S. Reactions of Molybdenum Pentachloride with Oxygen and Nitrogen Donor Ligands. *Polyhedron* **2013**, *61*, 188–194. https://doi.org/10.1016/j.poly.2013.06.001.
- (76) Wang, W.; Yang, F.; Chen, C.; Zhang, L.; Qin, Y.; Knez, M. Tuning the Conductivity of Polyaniline through Doping by Means of Single Precursor Vapor Phase Infiltration. *Advanced Materials Interfaces* **2017**, *4* (4). https://doi.org/10.1002/admi.201600806.
- (77) do Nascimento, G. M.; Sestrem, R. H.; Temperini, M. L. A. Structural Characterization of Poly-Para-Phenylenediamine-Montmorillonite Clay Nanocomposites. *Synthetic Metals* 2010, 160 (23–24), 2397–2403. https://doi.org/10.1016/j.synthmet.2010.09.016.
- (78) Sen, S.; Sarkar, P. A Novel Third-Generation Xanthine Biosensor with Enzyme Modified Glassy Carbon Electrode Using Electrodeposited MWCNT and Nanogold Polymer Composite Film. *RSC Advances* **2015**, *5* (116), 95911–95925. https://doi.org/10.1039/c5ra18889j.
- (79) Bailey, D. N.; Hercules, D. M.; Roe, D. K. Electrochemistry and Photopotentials of Phenazine in Methanol Solutions. *Journal of The Electrochemical Society* **1969**, *116* (2), 190. https://doi.org/10.1149/1.2411793.
- (80) Sawyer, D. T.; Komai, R. Y. Electrochemistry of Phenazine at a Platinum Electrode in Aprotic Solvents. *Analytical Chemistry* **1972**, *44* (4), 715–721. https://doi.org/10.1021/ac60312a002.
- (81) Trchová, M.; Stejskal, J. Resonance Raman Spectroscopy of Conducting Polypyrrole Nanotubes: Disordered Surface versus Ordered Body. *Journal of Physical Chemistry A* **2018**, *122* (48), 9298–9306. https://doi.org/10.1021/acs.jpca.8b09794.
- (82) Santos, M. J. L.; Brolo, A. G.; Girotto, E. M. Study of Polaron and Bipolaron States in Polypyrrole by in Situ Raman Spectroelectrochemistry. *Electrochimica Acta* **2007**, *52* (20), 6141–6145. https://doi.org/10.1016/j.electacta.2007.03.070.
- (83) Trchová, M.; Morávková, Z.; Bláha, M.; Stejskal, J. Raman Spectroscopy of Polyaniline and Oligoaniline Thin Films. *Electrochimica Acta* **2014**, *122*, 28–38. https://doi.org/10.1016/j.electacta.2013.10.133.
- (84) Stuart, C. M.; Frontiera, R. R.; Mathies, R. A. Excited-State Structure and Dynamics of Cis- and Trans-Azobenzene from Resonance Raman Intensity Analysis. *Journal of Physical Chemistry A* **2007**, *111* (48), 12072–12080. https://doi.org/10.1021/jp0751460.
- (85) Luo, C.; Borodin, O.; Ji, X.; Hou, S.; Gaskell, K. J.; Fan, X.; Chen, J.; Deng, T.; Wang, R.; Jiang, J.; Wang, C. Azo Compounds as a Family of Organic Electrode Materials for

- Alkali-Ion Batteries. *Proc Natl Acad Sci U S A* **2018**, *115* (9), 2004–2009. https://doi.org/10.1073/pnas.1717892115.
- (86) Yang, Y.; Teng, F.; Yu, L.; Liu, Y.; Song, P.; Xia, L. Isomerization of p, P'-Diiodoazobenzene Controlled by the Surface Plasmon-Assisted Reaction. *ACS Omega* **2019**, *4* (4), 7076–7081. https://doi.org/10.1021/acsomega.9b00429.
- (87) Bach, H. C.; Hinderer, H. E. Aromatic Azopolymers With Segments of Extended Conjugation. *Appl Polym Symp* **1973**, No. 2, 35–42.
- (88) Han, S.; Cheng, Y.; Liu, S.; Tao, C.; Wang, A.; Wei, W.; Yu, H.; Wei, Y. Selective Oxidation of Anilines to Azobenzenes and Azoxybenzenes by a Molecular Mo Oxide Catalyst. *Angewandte Chemie International Edition* **2021**, *60* (12), 6382–6385. https://doi.org/10.1002/anie.202013940.
- (89) Yadavalli, N. S.; Korolkov, D.; Moulin, J. F.; Krutyeva, M.; Santer, S. Probing Opto-Mechanical Stresses within Azobenzene-Containing Photosensitive Polymer Films by a Thin Metal Film Placed Above. *ACS Applied Materials and Interfaces* **2014**, *6* (14), 11333–11340. https://doi.org/10.1021/am501870t.
- (90) Bard, A. J.; Faulkner, L. R. *Electrochemical Methods: Fundamentals and Applications*, 2nd ed.; John Wiley & Sons: New York, NY, 2000. https://doi.org/0471043729.
- (91) Pavlishchuk, V. v.; Addison, A. W. Conversion Constants for Redox Potentials Measured versus Different Reference Electrodes in Acetonitrile Solutions at 25°C. *Inorganica Chimica Acta* **2000**, *298* (1), 97–102. https://doi.org/10.1016/S0020-1693(99)00407-7.
- (92) Ramanujam, P. S.; Johansen, P. M.; Hvilsted, S.; Pedersen, T. G. Quantum Theory and Experimental Studies of Absorption Spectra and Photoisomerization of Azobenzene Polymers. *JOSA B, Vol. 15, Issue 11, pp. 2721-2730* **1998**, *15* (11), 2721–2730. https://doi.org/10.1364/JOSAB.15.002721.
- (93) Yanguas-Gil, A.; Mane, A.; Elam, J. W.; Wang, F.; Severa, W.; Daram, A. R.; Kudithipudi, D. The Insect Brain as a Model System for Low Power Electronics and Edge Processing Applications. *Proceedings 2019 IEEE Space Computing Conference, SCC 2019* **2019**, 60–66. https://doi.org/10.1109/SpaceComp.2019.00012.
- (94) Kim, M. K.; Park, Y.; Kim, I. J.; Lee, J. S. Emerging Materials for Neuromorphic Devices and Systems. *iScience* **2020**, *23* (12), 101846. https://doi.org/10.1016/j.isci.2020.101846.
- (95) Kim, Y.; Kim, G.; Ding, B.; Jeong, D.; Lee, I.; Park, S.; Kim, B. J.; McCulloch, I.; Heeney, M.; Yoon, M. H. High-Current-Density Organic Electrochemical Diodes Enabled by Asymmetric Active Layer Design. *Advanced Materials* **2022**, *2107355*, 1–10. https://doi.org/10.1002/adma.202107355.
- (96) Kötz, R.; Carlen, M.; Ko, R.; Carlen, M. Principles and Applications of Electrochemical Capacitors. *Electrochimica Acta* **2000**, *45*, 2483–2498.

- (97) Liu, T.; Finn, L.; Yu, M.; Wang, H.; Zhai, T.; Lu, X.; Tong, Y.; Li, Y. Polyaniline and Polypyrrole Pseudocapacitor Electrodes with Excellent Cycling Stability. *Nano Letters* **2014**, *14* (5), 2522–2527. https://doi.org/10.1021/nl500255v.
- (98) Sabatani, E.; Redondo, A.; Rishpon, J.; Rudge, A.; Rubinstein, I.; Gottesfeld, S. Morphology Control in Electrochemically Grown Conducting Polymer Films. Part 2.— Effects of Cathodic Bias on Anodically Grown Films Studied by Spectroscopic Ellipsometry and Quartz-Crystal Microbalance. *J. Chem. Soc., Faraday Trans.* **1993**, *89* (2), 287–294. https://doi.org/10.1039/FT9938900287.
- (99) Huang, W. S.; Humphrey, B. D.; MacDiarmid, A. G. Polyaniline, a Novel Conducting Polymer. Morphology and Chemistry of Its Oxidation and Reduction in Aqueous Electrolytes. *Journal of the Chemical Society, Faraday Transactions 1: Physical Chemistry in Condensed Phases* **1986**, *82* (8), 2385–2400. https://doi.org/10.1039/F19868202385.
- (100) Barbero, C.; Miras, M. C.; Haas, O.; Kötz, R. Alteration of the Ion Exchange Mechanism of an Electroactive Polymer by Manipulation of the Active Site. Probe Beam Deflection and Quartz Crystal Microbalance Study of Poly(Aniline) and Poly(N-Methylaniline). *Journal of Electroanalytical Chemistry* **1991**, *310* (1–2), 437–443. https://doi.org/10.1016/0022-0728(91)85280-3.
- (101) Mao, X.; Liu, A.; Tian, W.; Wang, X.; Gleason, K. K.; Hatton, T. A. Enhancing Performance Stability of Electrochemically Active Polymers by Vapor-Deposited Organic Networks. *Advanced Functional Materials* **2018**, *28* (10). https://doi.org/10.1002/adfm.201706028.
- (102) Young, M. J.; Kiryutina, T.; Bedford, N. M.; Woehl, T. J.; Segre, C. U. Discovery of Anion Insertion Electrochemistry in Layered Hydroxide Nanomaterials. *Scientific Reports* **2019**, *9* (1), 2462. https://doi.org/10.1038/s41598-019-39052-1.
- (103) Arulrajan, A. C.; Ramasamy, D. L.; Sillanpää, M.; van der Wal, A.; Biesheuvel, P. M.; Porada, S.; Dykstra, J. E. Exceptional Water Desalination Performance with Anion-Selective Electrodes. *Advanced Materials* **2019**, *31* (10), 1–5. https://doi.org/10.1002/adma.201806937.
- (104) Gregory, S. A.; Hanus, R.; Atassi, A.; Rinehart, J. M.; Wooding, J. P.; Menon, A. K.; Losego, M. D.; Snyder, G. J.; Yee, S. K. Quantifying Charge Carrier Localization in Chemically Doped Semiconducting Polymers. *Nature Materials* **2021**, *20* (10), 1414–1421. https://doi.org/10.1038/s41563-021-01008-0.
- (105) Elam, J. W.; Groner, M. D.; George, S. M. Viscous Flow Reactor with Quartz Crystal Microbalance for Thin Film Growth by Atomic Layer Deposition. *Review of Scientific Instruments* **2002**, *73* (8), 2981–2987. https://doi.org/10.1063/1.1490410.

- (106) Dinh, H. N.; Ding, J.; Xia, S. J.; Birss, V. I. Multi-Technique Study of the Anodic Degradation of Polyaniline Films. *Journal of Electroanalytical Chemistry* **1998**, *459* (1), 45–56. https://doi.org/10.1016/S0022-0728(98)00286-1.
- (107) Stejskal, J.; Gilbert, R. G. Polyaniline. Preparation of a Conducting Polymer(IUPAC Technical Report). *Pure and Applied Chemistry* **2002**, *74* (5), 857–867. https://doi.org/10.1351/pac200274050857.
- (108) Kaiser, H.; Hamacher, K.; Kulasekere, R.; Lee, W. T.; Ankner, J. F.; DeFacio, B.; Miceli, P. F.; Worcester, D. L. Neutron Inverse Optics in Layered Materials. *Inverse Optics III* 1994, 2241 (July 1994), 78–89. https://doi.org/10.1117/12.179750.
- (109) *Reflpak* | *NIST*. https://www.nist.gov/services-resources/software/reflpak (accessed 2022-02-15).
- (110) Parratt, L. G. Surface Studies of Solids by Total Reflection of X-Rays. *Physical Review* **1954**, *95* (2), 359. https://doi.org/10.1103/PhysRev.95.359.
- (111) Fujiwara, H. *Spectroscopic Ellipsometry Principles and Applications*; John Wiley & Sons, Ltd: Tokyo, Japan, 2007. https://doi.org/10.1002/9780470060193.fmatter.
- (112) Sadrolhosseini, A. R.; Abdul Rashid, S.; Noor, A. S. M.; Kharazmi, A.; Lim, H. N.; Mahdi, M. A. Optical Band Gap and Thermal Diffusivity of Polypyrrole-Nanoparticles Decorated Reduced Graphene Oxide Nanocomposite Layer. *Journal of Nanomaterials* **2016**, *2016*, 1–8. https://doi.org/10.1155/2016/1949042.

For Table of Contents Only

